

Encapsulation and stabilization of indocyanine green within poly(styrene-alt-maleic anhydride) block-poly(styrene) micelles for near-infrared imaging

Victoria B. Rodriguez*

Scott M. Henry*

Allan S. Hoffman

Patrick S. Stayton

Xingde Li

Suzie H. Pun

University of Washington

Department of Bioengineering

Box 355061, William H. Foegle Building

Seattle, Washington 98195-5061

E-mail: xingde@u.washington.edu

Abstract. Indocyanine green (ICG) is a Federal Drug Administration-approved near-infrared imaging agent susceptible to chemical degradation, nonspecific binding to blood proteins, and rapid clearance from the body. In this study, we describe the encapsulation of ICG within polymeric micelles formed from poly(styrene-alt-maleic anhydride)-block-poly(styrene) (PSMA-b-PSTY) diblock copolymers to stabilize ICG for applications in near-infrared diagnostic imaging. In aqueous solution, the diblock copolymers self-assemble to form highly stable micelles approximately 55 nm in diameter with a critical micelle concentration (CMC) of ~ 1 mg/L. Hydrophobic ICG salts readily partition into the PSTY core of these micelles with high efficiency, and produce no change in micelle morphology or CMC. Once loaded in the micelle core, ICG is protected from aqueous and thermal degradation, with no significant decrease in fluorescence emission over 14 days at room temperature and retaining 63% of its original emission at 37°C. Free ICG does not release rapidly from the micelle core, with only 11% release over 24 h. The ICG-loaded micelles do not exhibit significant cell toxicity. This system has the potential to greatly improve near-infrared imaging in breast cancer detection by increasing the stability of ICG for formulation/administration, and by providing a means to target ICG to tumor tissue.

© 2008 Society of Photo-Optical Instrumentation Engineers. [DOI: 10.1117/1.2834296]

Keywords: indocyanine green; poly(styrene-alt-maleic anhydride)-block-poly(styrene) diblock copolymers; polymer micelles; stabilization; near-infrared imaging; tumor imaging.

Paper 07248R received Jul. 9, 2007; revised manuscript received Aug. 29, 2007; accepted for publication Sep. 14, 2007; published online Jan. 30, 2008.

1 Introduction

For deep tissue imaging, fluorescent contrast agents with excitation and emission in the near-infrared (NIR) range (~ 700 to 900 nm) are generally preferred as analytical and diagnostic tools compared with agents fluorescing in other regions, such as cyanine dyes (cy3 and cy5), green fluorescent proteins, and luciferin/luciferase reporter systems.^{1,2} The advantages of NIR contrast agents result from greater depth of light penetration within this part of the spectrum. An incident NIR light beam penetrating a tissue surface is subject to less absorption and optical scattering than incident visible (350 to 700 nm) or infrared light (>900 nm).³ In addition, autofluorescence background from tissues is minimal in the NIR region. NIR imaging therefore presents the advantages of greater sensitivity over other imaging modalities, as well as greater imaging depths, allowing tissue visualization depths up to several centimeters.¹ Optical imaging also eliminates exposure to ionizing radiation in contrast to conventional

methods of cancer screening such as mammography or positron emission tomography. Therefore, NIR contrast agents, including organic dyes, quantum dots, and polymeric fluorophores, are attractive materials for biomedical imaging with applications in early cancer screening beyond the skin, particularly breast cancer.

Indocyanine green (ICG) is a Federal Drug Administration (FDA)-approved NIR dye that belongs to the polymethine class of NIR contrast agents.⁴ ICG is used to visualize blood flow and clearance, with applications in monitoring cardiac output, liver function, and neovascularization or macular degeneration.⁵⁻¹⁰ The application of ICG imaging in early breast cancer detection has also been demonstrated based on the extravasation of ICG bound to blood proteins from leaky tumor vasculature.^{9,11-15} Although ICG has an advantageous excitation and emission spectrum, with a λ_{\max} of 775/831 nm (em/ex) in water and $\sim 800/840$ nm (em/ex) when bound to serum proteins,^{16,17} the use of ICG as a versatile contrast agent is limited by several properties. First, ICG is an unstable molecule susceptible to rapid aqueous, photo, and thermal instability.^{2,5} For example, the half-life of ICG in

*Equally contributing authors

Address all correspondence to Suzie Pun, Bioengineering University of Washington, Box 355061-1705 NE Pacific St., Seattle, WA 98195; Tel: 206 685 3488 FAX: 206 616 3928; E-mail: spun@u.washington.edu

aqueous solution is 16.8 ± 1.5 h at room temperature in the dark and decreases significantly at physiological temperatures and with exposure to light.² Degradation of ICG in aqueous solution is due to interactions with solvent radicals and ions leading to saturation of the carbon double-bonded chain and the formation of leucoforms (reduced, nonfluorescent forms of the dye molecule).^{2,18} These leucoforms and other fragments are incapable of excitation and emission in the near-infrared portions of the spectrum. During light exposure, solvent radicals and ions along with radicals formed from photoexcited ICG accelerate the degradation process; when aqueous ICG is exposed to increased temperatures, the degradation process is accelerated in the same manner due to increased kinetics of radical formation.^{2,18} Second, after administration, ICG exhibits nonspecific binding to blood proteins with a high affinity toward α_1 lipoproteins.^{5,16} Finally, ICG is cleared rapidly from the body with a biphasic plasma clearance consisting of a fast initial half life of 3 to 4 min and a slow half life above one hour at low concentrations.^{2,5,19} Thus, formulations of ICG that provide increased chemical stability, protection from nonspecific protein binding, and enhanced circulation time are critical for expanding the repertoire of potential applications for this dye.

Polymeric nanoparticles (defined as 1 to 1000 nm in size) have been used as delivery vehicles for various therapeutic and imaging applications.²⁰ Compared to free drug or imaging agents, nanoparticulate formulations present several advantages, including targeting capabilities and protection of therapeutic cargo against degradation or rapid clearance from the body. Polymeric nanoparticles passively target solid tumors due to the increased endocytotic activity, porous vasculature, and poor lymphatic drainage characteristic of these tissues, a phenomenon known as the enhanced permeation and retention (EPR) effect.²¹⁻²³ Additionally, polymeric carriers can be functionalized to include active targeting ligands or to prolong circulation time.²¹ Recently, Saxena et al. incorporated ICG into poly(lactic-co-glycolic acid) (PLGA) nanoparticles and demonstrated significantly enhanced photo, thermal, and aqueous stability of ICG compared to free ICG.²⁴ In particular, encapsulation of ICG within the nanoparticle resulted in a degradation half life 4.3 times greater than that of free ICG when observed over a four day period at 22°C in the dark.²⁴ In a different study, Yu et al. developed silica/polymer capsules containing ICG for photothermal applications.²⁵ These formulations also imparted photostability to encapsulated ICG. However, both of these ICG carriers would likely have limited utility for imaging of metastatic cancer due to particle sizes that are near or greater than the upper limit of fenestrations observed in tumor vasculature (mean diameter of approximately 360 nm for the PLGA nanoparticles and 0.6 to 2 μm for the silica/polymer capsules).²⁴⁻²⁶

The goal of our work is to develop a nanoparticulate delivery system for ICG that provides efficient dye loading, stabilized fluorescence over long time periods, potential chemistries for functionalization, and dimensions amenable to systemic delivery. The development of such a system will greatly improve the utility of ICG for early detection of breast cancer by increasing the stability of ICG and by providing a means to target ICG to tumor tissue. Here, we describe the synthesis, formulation, and characterization of ICG-

containing polymeric micelles. Our results suggest that these materials protect ICG against degradation, without adversely impacting its spectral properties. Additionally, the micelle size and stability are ideally suited for passive targeting of ICG encapsulated micelles to the tumor milieu, and the polymer chemistry employed is readily adaptable for the incorporation of active targeting ligands.

2 Materials and Methods

2.1 Materials

All chemicals were purchased from Sigma-Aldrich (Milwaukee, Wisconsin) and used without further purification unless otherwise noted. The free radical initiator 2,2'-azo-bis(isobutyronitrile) (AIBN) was recrystallized from methanol prior to use. Styrene was purified by distillation under reduced pressure. Maleic anhydride was recrystallized from chloroform. Solvents used were ACS grade and obtained from Sigma-Aldrich with the exception of ethyl ether (EMD, Gibbstown, New Jersey).

2.2 Polymer Synthesis

Poly(styrene-alt-maleic anhydride)-block-poly(styrene) (PSMA-b-PSTY) copolymers were prepared by a thermally initiated, two-step reversible addition-fragmentation chain transfer (RAFT) polymerization using the chain transfer agent (CTA) S-benzylthiobenzoate (BDTB). BDTB was prepared from S-(thiobenzoyl)thioglycolic acid and benzylmercaptan as previously described.²⁷ In the first step, equimolar amounts of styrene and maleic anhydride (0.03 mol) were polymerized for 18 h at 60°C with AIBN as initiator and BDTB (0.00075 mol) as chain-transfer agent in p-dioxane (50 wt%). The BDTB:AIBN ratio was 10:1, and the polymerization vessel was subject to three cycles of freeze-vacuum-thaw before polymerization. The PSMA macro-CTA (Mn 9700 kDa, PDI=1.34) was isolated by precipitation in ethyl ether, filtered, and dried under vacuum at room temperature. In the second step, 1.9130 g of macro-CTA were combined with 0.033-mol styrene and 3.23-mg AIBN (10:1 macro-CTA:initiator ratio) in dimethylformamide (DMF) (36 wt%) in a round bottom flask. The solution was degassed by three cycles of freeze-vacuum-thaw, and polymerization was carried out for 24 h in a 60°C oil bath. The block copolymer PSMA-b-PSTY (Mn 21,600 kDa, PDI=1.31) was recovered by precipitation in ethyl ether, followed by filtration, and dried under vacuum at room temperature.

The molecular weights of the PSMA macro-CTA and PSMA-b-PSTY block copolymers were determined by size exclusion chromatography using Tosoh TSK-GEL α -3000 and α -4000 columns (Tosoh Bioscience, Montgomeryville, Pennsylvania) connected in series to a Viscotek GPCmax VE2001 and refractometer VE3580 (Viscotek, Houston, Texas). High pressure liquid chromatography (HPLC)-grade DMF containing 0.1 wt% LiBr was used as the mobile phase. The molecular weights of the synthesized copolymers were determined using a series of poly(methyl methacrylate) standards.

Following synthesis of the PSMA-b-PSTY block copolymer, the PSMA block was derivatized with butylamine as previously described,²⁸ yielding a pH-sensitive hydrophilic

PSMA derivative through aminolysis of 60% of the anhydride groups in the PSMA block. Briefly, a solution of PSMA-b-PSTY block copolymer (13 wt%) was prepared in DMF. Subsequently, 1 mL of a 0.33-M solution of butylamine in DMF was added drop-wise while stirring, and the solution was allowed to react for 24 h at room temperature. The polymer was recovered by precipitation in ethyl ether, and remaining anhydrides were hydrolyzed by dissolving the polymer in 1-N NaOH. After 3 h, the solution was extensively dialyzed against deionized water using SpectraPor Slide-a-Lyzer cassettes (MWCO=3500, Pierce, Rockford, Illinois) to remove sodium salts and neutralize the solution prior to lyophilization.

2.3 Micelle Formation

Modified PSMA-b-PSTY block copolymers (37.3 mg) were dissolved in 6-mL DMF and 360- μ L 1-N NaOH (6 vol%). After 30 min of stirring, 6 mL of nanopure H₂O (pH 9) was added by syringe pump at a rate of 20 μ L/min. Following injection, the solution was transferred to a dialysis cassette (MWCO 3500, Pierce) and dialyzed extensively against nanopure H₂O. Following dialysis, the solution was filtered through a 0.2- μ m filter.

2.4 Indocyanine Green Encapsulation

A solvent evaporation method was employed to encapsulate ICG into the micelles after complexing ICG with tetrabutylammonium iodide to form a hydrophobic ICG-tetrabutylamine salt. Briefly, a 1-mM solution of ICG was prepared in chloroform with a six-fold molar excess of tetrabutylammonium iodide. The solution was sonicated for 30 min, then diluted in chloroform to obtain a final ICG concentration of 260 μ M. The chloroform ICG solution was then added to a stirring micelle solution (2.1 mg/mL), yielding a final ICG concentration of 10- μ M ICG. The chloroform was removed by evaporation, causing ICG to partition into the hydrophobic cores of the PSMA-b-PSTY micelles. Free ICG was then separated from the ICG-micelle solutions using Amicon regenerated cellulose centrifuge filters (MWCO 100 kDa, Millipore, Billerica, Massachusetts). Following ultrafiltration, the micelle-ICG solution was rinsed three times using nanopure H₂O. The carryover volume between rinses was less than 100 μ L. Purified micelles were resuspended in the original volume of nanopure H₂O. The final micelle concentration after filtering was determined by ¹H-NMR. Lyophilized samples were resuspended in deuterated DMF containing 1% trimethylsilane (TMS). Concentration was determined by comparing the styrenic peak area to a series of known standards using the TMS peak as an internal reference standard.

2.5 Characterization

2.5.1 Indocyanine green loading efficiency

The efficiency of ICG loading was determined by lyophilizing 1-mL samples of micelle-encapsulated ICG solutions. After drying, the micelle solutions were dissolved in dimethylformamide (DMF), causing complete dissolution of the micelle and release of the encapsulated ICG. The ICG concentration was determined by comparing ICG absorbance at 775 nm to a

standard curve of free ICG dissolved in DMF. The loading efficiency was then determined by the ratio of micelle-associated ICG to total ICG. The total ICG mass was defined as the amount of ICG initially added to the micelle solutions during encapsulation. All loading measurements were performed in triplicate.

2.5.2 Size, charge, and morphology of micelles

The size distribution of the micelles was determined before and after ICG loading by dynamic light scattering (DLS) in water and phosphate buffered saline 1 \times (PBS 1 \times , NaCl concentration of 154 mM) using a Brookhaven (Holtsville, New York) BI90Plus instrument equipped with a 535-channel correlator. A 656-nm laser source was used as the incident beam, and measurements were performed at a 90-deg angle. Calculations of particle diameter distributions were performed by the method of cumulants analysis. For unloaded and loaded micelles in PBS 1 \times , the size was also examined 50 min after dilution in buffer to observe micelle salt stability. Zeta potential analysis was also performed on unloaded and loaded micelles in water using the Brookhaven BI90Plus. Atomic force microscopy (AFM) was used to determine micelle morphology and confirm the micelle size. A dilute solution (10 ng/ μ L) of micelle-encapsulated ICG in water was applied on the surface of a cleaved mica disk (Ted Pella, Incorporated, Redding, California) and allowed to dry overnight. The mica surface was then rinsed with water and dried with nitrogen gas prior to AFM analysis. AFM scans of the micelle-coated mica surface were recorded and analyzed on a digital multimode AFM with Nanoscope IIIa controller (Veeco Instruments Incorporated, Woodbury, New York).

2.5.3 Critical micelle concentration

The critical micelle concentration (CMC) is the minimum concentration at which monomeric polymers dispersed in solution organize to form micelles. The CMC of the PSMA-b-PSTY system was investigated by observing the solvatochromic shift in fluorescence emission of 6-propionyl-2-(dimethylamino)naphthalene (PRODAN, Molecular Probes, Eugene, Oregon) as a function of block copolymer concentration. Following previously described protocols,²⁹ a solution of PRODAN dye at 2.4×10^{-5} M in methanol was aliquoted into a series of glass vials. The vials were protected from light and dried under vacuum. Next, PSMA-b-PSTY solutions were added to the dry vials in triplicate at concentrations ranging from 0.4 mg/mL to 1×10^{-7} mg/mL and allowed to stand overnight in the dark. The next day, the solutions were transferred to a 96-well polystyrene plate for fluorescence assays (Costar, Corning Incorporated, Lowell, Massachusetts) and read for PRODAN emission with excitation at 360 nm (15-nm bandwidth) and emission scan from 400 to 600 nm (5-nm bandwidth) on a Sapphire 2 fluorescent microplate detector (Tecan, Austria). The CMC was determined by plotting the ratio of the peak hydrophobic emission intensity (436 nm) to the peak hydrophilic emission intensity (518 nm) against the polymer concentration on a logarithmic scale. From this plot, the CMC was determined as the concentration at which the curve of the hydrophobic/hydrophilic ratio begins to increase with polymer concentration.

2.6 Formulation and Stability

2.6.1 Aqueous and thermal stability studies

The solution stability and thermal stability of ICG encapsulated within polymeric micelles were determined by assessing ICG emission over a three week period. For each reading, micelle-encapsulated ICG solutions were plated in triplicate into a 96-well plate. The emission intensity of the encapsulated ICG from 786 to 850 nm (bandwidth 5 nm) was measured on the Tecan microplate detector using an excitation of 775 nm (bandwidth 5 nm). All settings, such as the gain, integration time, number of reads, read position on plate, z-position of the scanner, and temperature, were maintained constant for the duration of the study. The fluorescence emission of ICG was recorded frequently within the first 24 h, approximately every 24 h for the next two weeks, and every 100 h within the third week. Controls consisted of free ICG in water prepared from the same stock as the encapsulated ICG, and unloaded micelles. For storage between readings, solutions were sealed in a glass vial and maintained in the dark at room temperature, or in a 37°C oven for the solution and thermal stability study, respectively. For analysis, normalized ICG emission was determined using the maximal emission intensity within a 10-nm spectral bandwidth for each sample at a given time compared to the corresponding ICG emission at time zero. The average normalized emission intensity for each triplicate sample set was plotted as a function of time.

2.6.2 Kinetics of indocyanine green release from micelles

Release of ICG from freshly loaded polymeric micelles was examined for a period of 24 h. First, 1.5-mL samples of ICG-encapsulated micelle solution were added to 25K MWCO dialysis tubing (SpectraPor, Spectrum® Labs, Incorporated, Rancho Dominguez, California), and the samples were dialyzed against 1 L of H₂O. During the study, the samples were stored in the dark at 4°C. At specified time points, fractions were collected from the solution within the dialysis tubing, and the remaining ICG concentration was determined by examining the absorbance of ICG at 775 nm. A control consisted of free ICG. All measurements were performed in triplicate. The fraction of release was determined by comparing the ICG concentration found in each sample to that initially loaded.

2.7 In Vitro Study—Cytotoxicity and IC₅₀ Value Determination

The IC₅₀ (concentration of material that induces 50% cell death) of PSMA-b-PSTY micelles encapsulating ICG was determined using the MTS tetrazolium salt (3-(4,5-dimethylthiazol-2-yl)-5-(3-carboxymethoxyphenyl)-2-(4-sulfophenyl)-2H-tetrazolium salt) metabolic assay on NIH-3T3 cells. Cells were seeded at 12,000 cells/well in a 96-well tissue culture polystyrene plate (Costar Corning Incorporated Lowell Massachusetts). The cells were allowed to adhere to plates overnight prior to addition of micelle solutions. Stock micelle solutions at 2.1 mg/mL were sterilized by filtration through a 0.2-μm syringe filter, diluted in cell culture media to final concentrations of 0.3, 0.6, 1.1, and 1.7 mg/mL, then added to cells. The cells were incubated in the presence of

micelle solutions for 4.5 h in the incubator. The media was then replaced with fresh media, and the cells were returned to the incubator for 24 h. At the conclusion of the 24 h incubation, the cells were rinsed and treated with MTS reagent following manufacturer's specifications (CellTiter 96® AQ_{ueous} MTS Reagent Powder, Promega Corporation Madison, Wisconsin). Cell viability was evaluated by recording the absorbance of each well at 490 nm using a microplate reader. Positive controls consisted of cells exposed to the same water/media concentration as each micelle treatment, and a negative control consisted of cells exposed to 0.5-mg/mL branched-polyethylenimine (b-PEI, MW 25K, Sigma, Saint Louis, Missouri).

3 Results

3.1 Polymer Synthesis and Micelle Characterization

Block copolymers of poly(styrene-alt-maleic anhydride)-block-poly(styrene) (PSMA-b-PSTY) were successfully prepared with controlled architectures and low polydispersities using a two-step RAFT polymerization. Following polymerization, the maleic anhydride groups of the PSMA block were subject to ring-opening aminolysis using butylamine to obtain an amphiphilic copolymer as previously described (Fig. 1).²⁸ 60% of the maleic anhydride residues were opened by aminolysis with butylamine, followed by base-catalyzed hydrolysis to open the remainder of the maleic anhydride moieties. These modifications yield a block copolymer with a hydrophobic poly(styrene) component and hydrophilic poly(styrene-alt-maleic anhydride) component. The copolymers self-assemble in aqueous environments to form polymeric micelles with hydrodynamic diameters of 55 ± 2.7 nm as determined by dynamic light scattering. In addition, the overall charge of the micelles was determined to be near-neutral by zeta potential measurements (Table 1).

3.2 Indocyanine Green Encapsulation and Characterization

ICG was converted to the hydrophobic tetrabutylammonium salt and loaded into the hydrophobic micelle core by solvent evaporation. The efficiency of ICG loading was determined by computing the ratio of ICG concentration after loading to that of total ICG loaded, and was found to be 87 ± 5%. Next, the absorbance and fluorescence spectra of ICG were compared to the spectra of micelle-encapsulated ICG [Figs. 2(a) and 2(b), respectively]. Slight red-shifts were observed in both the absorbance and emission spectra of encapsulated ICG (25 and 10 nm, respectively).

The average diameter of ICG-loaded micelles was determined to be 30 ± 3.1 nm by dynamic light scattering. The overall charge of ICG-loaded micelles remained near-neutral (zeta potential of -0.11 ± 2.2 mV). Particle sizing experiments revealed excellent salt stability of the empty and ICG-loaded micelles with minimal size change observed after 50 min of incubation in phosphate buffered saline containing 150-mM NaCl. The particle characterization data are reported in Table 1. Micelle size and morphology were also determined by AFM after ICG loading. The AFM imaging of these particles showed an average diameter of 30.8 nm ± 2.5 nm (Fig. 3). Atomic force microscopy also revealed an overall spheri-

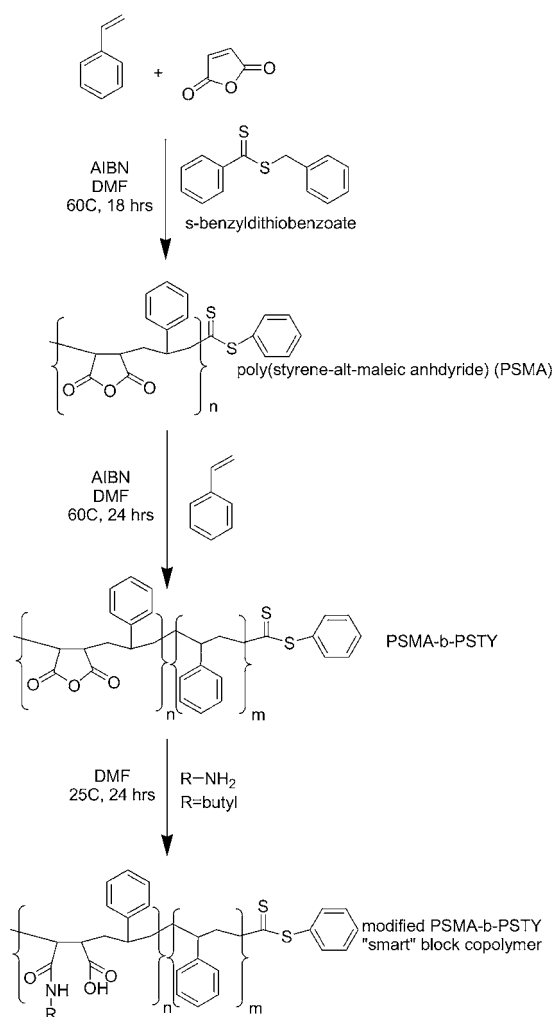


Fig. 1 Schematic of poly(styrene)-block-poly(styrene-alt-maleic anhydride) (PSMA-b-PSTY) diblock copolymer synthesis, the building block for the polymeric micelle to encapsulate ICG.

cal morphology, though it appeared the micelles flattened on the mica surface with the height of each individual particle smaller ($4.40 \text{ nm} \pm 0.34 \text{ nm}$) than its width along the surface. Based on the combined AFM and DLS data, it is reasonable to speculate that the micelles deform during the drying process before AFM imaging.

The critical micelle concentration (CMC) is an indication of micelle stability, a critical parameter for micelle-based therapeutics. Generally, the lower the CMC, the more stable

the micelle. The CMC of the PSMA-b-PSTY micelles was determined both before and after loading ICG by measuring the solvatochromic shift of PRODAN fluorescence emission as a function of polymer concentration (Fig. 4). Above the CMC, PRODAN partitions from aqueous solution into the hydrophobic cores of polymeric micelles, undergoing a significant blueshift relative to its emission in water.²⁹ Based on this method, the CMC of the PSMA-b-PSTY micelles alone was determined to be 1 mg/L. The CMC for the ICG loaded micelles was also determined to be 1 mg/L; thus, ICG loading does not affect the CMC of PSMA-b-PSTY micelles (Table 1).

3.3 Solution Stability, Thermal Stability, and Release of Encapsulated Indocyanine Green

To determine whether encapsulation in polymeric micelles could protect ICG from degradation, the aqueous stability of ICG in micelle formulations was investigated. The fluorescence emission of micelle-encapsulated ICG and free ICG was examined over a period of three weeks with measurements repeated approximately every 24 h for the first two weeks and every 100 h within the third week. The emission profile of ICG over time provides a strong indicator of its overall stability in a given environment, and is a key parameter for imaging applications. In these studies, the fluorescence emission of free ICG decreased rapidly over time, while the fluorescence emission intensity of micelle-encapsulated ICG remained constant throughout the two week duration of the study (Fig. 5). The emission of free ICG decreased to 50% of its original value within 96 h, and was reduced by more than 90% within 12 days. These findings are consistent with the rapid instability of free ICG reported in the literature.^{2,24,25} In contrast, no change in ICG emission was observed when ICG was encapsulated in the micelle core.

Free ICG also degrades rapidly at elevated temperatures, another significant limitation for *in vivo* imaging applications. To evaluate the thermal stability of ICG-encapsulated polymeric micelles compared to free ICG, fluorescence emission of ICG at physiological temperatures was recorded from samples stored in a 37°C oven over a period of three weeks. Emission of ICG was recorded at the same intervals as in the solution stability study. At 37°C, the emission of free ICG decreased rapidly to 17% within 96 h and 0% within six days (Fig. 5). In contrast, ICG encapsulated in micelles was relatively protected from thermal degradation, maintaining 97% of original emission for 96 h. In addition, after three weeks of incubation at 37°C, encapsulated ICG still showed 41% of its

Table 1 CMC, zeta potential, and particle sizing of unloaded and ICG-loaded micelles.

Polymeric micelle state	CMC (mg/L)	Zeta potential (mV)	Solvent for sizing	Size (nm, freshly prepared)	Size (nm, 50 min after prepared)
Unloaded	1	-1.32 ± 1.7	Water	55 ± 2.7	×
			PBS 1×	41 ± 1.5	40 ± 0.3
Loaded w/ICG	1	-0.11 ± 2.2	Water	30 ± 3.1	×
			PBS 1×	25 ± 2.1	24 ± 2.3

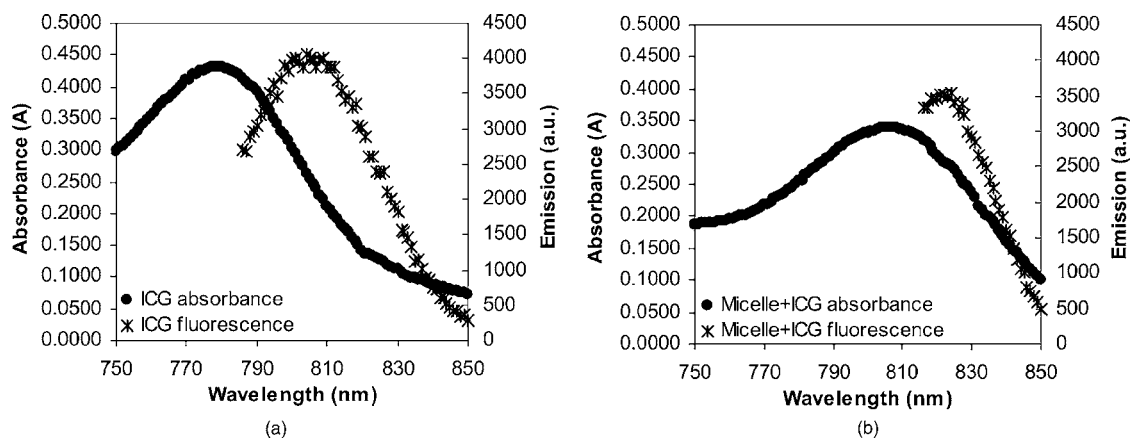


Fig. 2 Absorbance/emission spectra of (a) ICG and (b) micelle-encapsulated ICG. For fluorescence spectra, ICG and micelle-encapsulated ICG were excited at their respective maximum absorption wavelengths.

initial emission. These results demonstrate the stabilization of micelle-encapsulated ICG at both room temperature and physiological temperature.

For *in vivo* imaging applications, the micelles must retain ICG until they have reached the appropriate targeted tissue, and must protect ICG from degradation and clearance until imaging is complete. The release of ICG from polymeric micelles was examined by measuring the retention of ICG within dialysis tubing as a function of time. Solutions of micelle-encapsulated ICG and free ICG were dialyzed against a MWCO 25K membrane in deionized water for 24 h at 4 °C. At various time points, solutions were removed from the tubing, weighed, and concentrations of ICG remaining determined by absorbance readings at 775 nm. By determining the concentration of ICG remaining in the dialysis tubing at a given time point relative to the initial absorbance, the mass

loss of ICG was calculated as a percentage of the initial loading (Fig. 6). After 24 h, more than $89 \pm 6.8\%$ of the micelle-encapsulated ICG was retained in the tubing (i.e., 11% release), compared to $27 \pm 3.6\%$ remaining of free ICG (i.e., 73% release). This result indicates that the rate of ICG release from the micelles is sufficiently slow for *in vivo* imaging applications.

3.4 Cytotoxicity and IC_{50} Value Determination

A cytotoxicity study was performed to determine cell viability when exposed to increasing concentrations of micelle-encapsulated ICG. The IC_{50} , or concentration of polymer resulting in 50% cell death, was determined as an indicator of the toxicity of the polymeric micelles. Cell viability was determined by the MTS metabolic activity assay. No significant

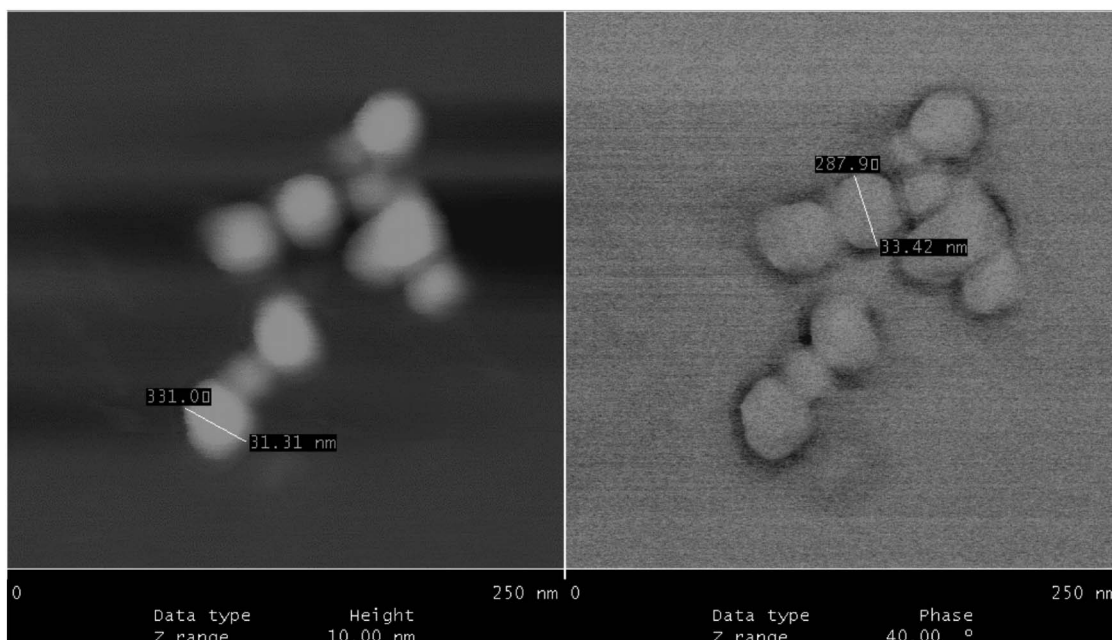


Fig. 3 Atomic force microscopic (AFM) image of polymeric micelles encapsulating indocyanine green (ICG). Flattened surface image is displayed at right, and at left, the image is displayed at a height of 10 nm.

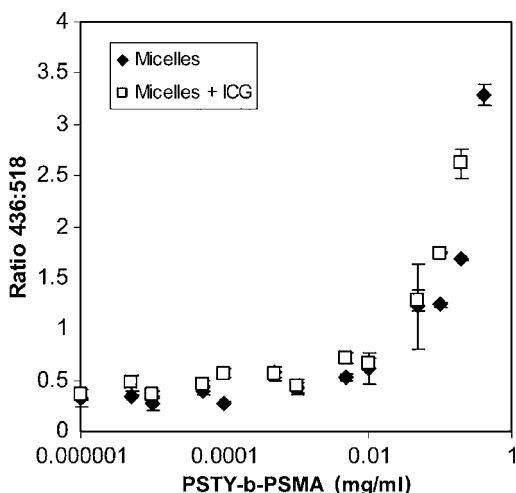


Fig. 4 The ratio of hydrophobic:hydrophilic PRODAN fluorescence emission (in nanometers) as a function of polymer concentration. Above the CMC, micelle formation causes an increase in the emission ratio as PRODAN partitions from aqueous solution into the hydrophobic micelle cores, undergoing a significant solvatochromic blueshift in fluorescence emission (436 to 518 nm).

cytotoxicity compared to control treatments was observed at concentrations of 0.3, 0.6, and 1.1 mg/mL of PSMA-b-PSTY. Increasing toxicity with polymer concentration between 1.1 to 1.7 mg/mL (the highest concentration provided) was observed with cell viability decreasing from 88 to 33%, respectively, indicating an IC_{50} of ~ 1.5 -mg/mL PSMA-b-PSTY (Fig. 7).

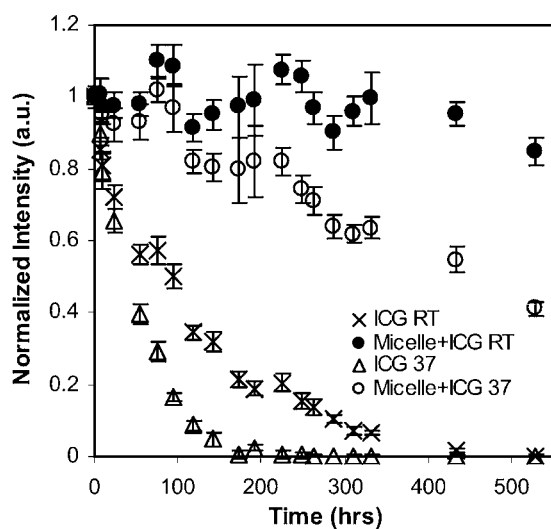


Fig. 5 Relative fluorescence emission of free ICG and micelle-encapsulated ICG over a three week period at room temperature (RT on legend) and 37°C (37 on legend). Solutions were maintained at the respective temperature and covered from light. Emission intensities were normalized to maximum fluorescence intensity within each sample at 0 h.

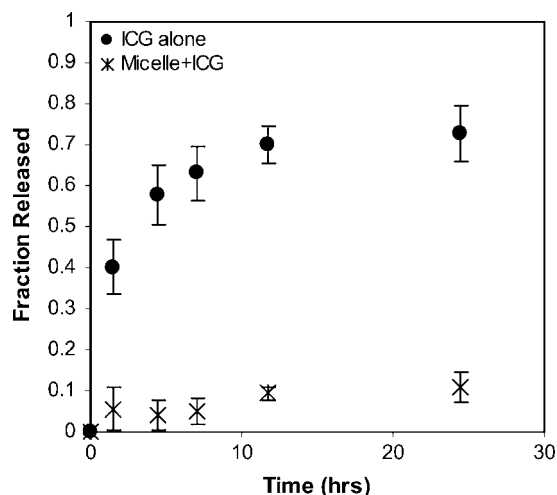


Fig. 6 Fraction of ICG released from dialysis bags over a 24-h period. Solutions of free ICG and micelle-encapsulated ICG were evaluated.

4 Discussion

4.1 Polymer Synthesis and Characterization

Previous studies have demonstrated the feasibility of one-pot synthetic procedures to prepare PSTY-b-PSMA block copolymers for the formation of micelles and cross-linked nanoparticles.^{30,31} However, a two-step synthesis was employed here for ease of characterization of the molecular weight and polydispersity of each block in the copolymer. These block copolymers self-assemble to form polymeric micelles. Advantages of these specific micelles include the PSTY glassy core that contributes to micelle stability (low CMC), and the presence of functional groups in the corona that can be used for future derivitization with targeting ligands. The formulated micelles also have ideal sizes for tumor imaging applications. The desired size of nanoparticles for delivery from leaky tumor vasculature is less than 400 to 600 nm.²⁶ In addition, particles less than 100 nm have

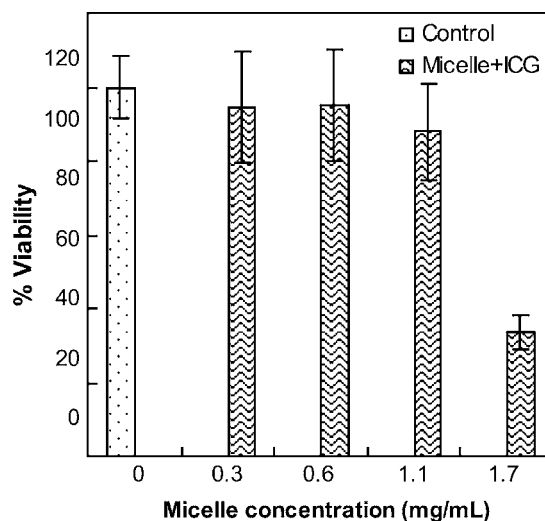


Fig. 7 Percent NIH-3T3 cell viability in response to exposure of cells to increasing concentrations of micelles encapsulating ICG.

decreased recognition by the reticuloendothelial system, resulting in longer circulation half lives.³² Prolonged circulation and reduced clearance will improve passive targeting to tumor tissue via the EPR effect. Unloaded micelles have an average diameter of 55 ± 2.7 nm, whereas ICG-loaded micelles have an average diameter of 30 ± 3.1 nm. The difference in size for the ICG-loaded micelles as opposed to the unloaded micelles is due to the process of ICG loading, not filtration, as was discovered in a separate study (data not shown). It is possible that the presence of chloroform during ICG loading allows reorganization of the micelle core. In physiologic salt concentrations, the sizes of both unloaded and loaded micelles were shown to be stable. The decrease in micelle hydrodynamic diameter after salt addition may be attributed in part to the salt shielding the anionic charges of PSMA polymers in the micelle corona, thereby decreasing electrostatic repulsion between the PSMA chains. In an *in vivo* setting, the micelles should be capable of maintaining their overall structure and thus retain cargo for circulation to the targeted site.

4.2 Indocyanine Green Encapsulation and Characterization

Tumor imaging using ICG is limited by the poor biodistribution and instability of the free dye. Recently, micelles have garnered great interest as carriers for therapeutic molecules because of their ability to improve the biodistribution and retention of small molecules, and their ability to protect fragile molecules during systemic circulation.³² By loading ICG into the cores of polymeric micelles, we hypothesized that the dye would be protected from rapid aqueous and thermal degradation without compromising the attractive spectral properties of the dye. To investigate this hypothesis, micelles derived from modified PSMA-b-PSTY block copolymers were loaded with ICG using a solvent evaporation method, which allowed ICG to partition into the hydrophobic micelle core. Using this method, ICG loading efficiencies of 87% were obtained from 10- μ M ICG loading solutions.

In aqueous solutions, free ICG is known to self-quench at concentrations above 5 μ M.^{12,33} Therefore, self-quenching of ICG in the micelle core was a potential concern. To investigate the effects of ICG concentration on ICG fluorescence in the polymeric micelle, various concentrations of ICG were loaded into the micelles, and the fluorescence emission intensity was compared (data not shown). These studies showed micelle-ICG fluorescence increased as the ICG concentration in the loading solution was changed from 5 to 10 μ M, but decreased with further increases in ICG concentration. Based on these results, an initial ICG loading of 10 μ M into polymeric micelles was taken as the optimal concentration.

The ICG loading efficiency obtained in our studies compares favorably with previously published results. In other systems, drug loading efficiencies in polymeric micelles have been reported between 10 and 90%.^{34–38} In this study, the hydrophobic tetrabutylamine salt of ICG was loaded with 87% efficiency. A recent study by Saxena et al. examined the stability of ICG when incorporated into PLGA nanoparticles, and calculated a $74.5 \pm 2.2\%$ loading efficiency.²⁴ Also, Yu et al. reported loading efficiencies between 90.0 and 97.1% when ICG was incorporated into much larger 0.6 to 2- μ m polymer nanoparticle-assembled capsules.²⁵ In comparison to

these previous studies, we can conclude that the ICG loading method we describe is highly efficient. Unlike previous investigations with ICG, we used tetrabutylammonium iodide to increase the hydrophobicity and micelle loading of ICG. The amount of tetrabutylammonium iodide used to form the ICG salt is 2300-fold below the LD₅₀ (oral in rat is 1990 mg/kg), and should not pose complications for *in vivo* imaging applications.³⁹

The stability of the polymeric micelles was determined by measuring the CMC before and after encapsulating ICG. Highly stable polymeric micelles (those with low CMCs) are required for *in vivo* applications, as micelles are subjected to significant dilution following intravenous injection.³² If injection reduces the block copolymer concentration below the CMC, polymeric micelles become thermodynamically unstable and begin to dissociate into component unimers. Dissociation is a kinetic process that occurs at different rates depending on the plasticity of the micelle core and other factors, but complete dissociation results in a loss of the therapeutic cargo. The CMC of the polymeric micelles described here was determined to be 1 mg/L for both unloaded micelles and ICG loaded micelles. This value is lower⁴⁰ or comparable^{41,42} to that reported by other micelles derived from various amphiphilic block copolymers. The stability of the polymeric micelle system we describe is a result of the high glass transition temperature T_g of the styrenic core, as has been well documented in previous work.³² For dosing in a mouse model, typical administration of ICG ranges from 0.2 to 0.4 mg/kg body weight.^{19,43} This value corresponds to 69 mg of micelles per kg or 1.2 mg per mL blood volume (assuming mouse blood volume is 5 to 6% body weight). Therefore, the target dose will be above the CMC of 1 mg/L by almost three orders of magnitude.

4.3 Solution Stability, Thermal Stability, and Release of Encapsulated Indocyanine Green

A recent study examined the stability of ICG when incorporated into PLGA nanoparticles.²⁴ ICG encapsulated in PLGA nanoparticles was stable after a four-day incubation in distilled water, showing 60% decrease in ICG fluorescence compared with free ICG (97.8% decrease).²⁴ In the system presented here, micellar formulations of ICG resulted in sustained stabilization of ICG based on peak fluorescence for more than two weeks without any significant degradation. This reflects the polymeric micelles' ability to stabilize ICG in an aqueous environment, thus allowing for easier formulation, longer shelf life, and a greatly enhanced diagnostic/therapeutic window. The micellar formulations of ICG also exhibited stability at 37°C; fluorescence intensity decreased by only 59% after three weeks incubation in solution at physiological temperatures.

Over time, ICG is expected to release from the micelles as it diffuses out of the polystyrene cores. However, because of the glassiness of the poly(styrene) cores, we anticipated that the rate of ICG release would be very slow. The actual release rate of ICG from the micelle cores was determined to be 11% over 24 h. It should be noted that for the free ICG control, ~60% of ICG released as a burst from the dialysis tubing within the first six hours, followed by a period of slower release, resulting in a 73% total loss after 24 h. The plateau of

release observed is likely due to fouling of the dialysis membrane by the released ICG. These results indicate the micelle-ICG formulation is sufficiently stable to allow for reasonable storage times and long imaging windows following *in vivo* administration.

5 Conclusions

In the present study, we show the encapsulation of ICG within polymeric micelles formed from poly(styrene-alt-maleic anhydride)-block-poly(styrene) (PSMA-b-PSTY) diblock copolymers. Characterization of the system shows efficient ICG loading, stabilized ICG fluorescence over varied conditions and long time periods, and minimal cytotoxicity. The polymeric micelle is capable of long-term retention of ICG, possesses a low CMC, and is readily adaptable for the incorporation of active targeting ligands. The PSMA-b-PSTY micelle system we discuss has the potential to greatly improve near-infrared imaging and detection of breast cancer by increasing the stability of ICG for formulation/administration, and by providing a means to target ICG to tumor tissue.

Acknowledgments

AFM studies were performed at the Nanotech User Facility, a member of the National Nanotechnology Infrastructure Network (NNIN), which is supported by the National Science Foundation and the Center for Nanotechnology at the University of Washington. We are grateful for the assistance of Xiangchun Yin, Adelaide Warsen, and Daniel MacDonald. This work was supported by an NSF Career Award (Li), the National Institutes of Health (R01 EB2991), University of Washington start-up funds (Pun), and a Ford Foundation Diversity Fellowship (Rodriguez).

References

1. K. Licha and C. Olbrich, "Optical imaging in drug discovery and diagnostic applications," *Adv. Drug Delivery Rev.* **57**(8), 1087–1108 (2006).
2. V. Saxena, M. Sadoqi, and J. Shao, "Degradation kinetics of indocyanine green in aqueous solution," *J. Pharm. Sci.* **92**(10), 2090–2097 (2003).
3. A. Zaheer, R. Lenkinski, A. Mahmood, A. Jones, L. Cantley, and J. Frangioni, "In vivo near-infrared fluorescence imaging of osteoblastic activity," *Nat. Biotechnol.* **19**(12), 1148–1154 (2001).
4. J. Rao, A. Dragulescu-Andrasi, and H. Yao, "Fluorescence imaging *in vivo*: recent advances," *Curr. Opin. Biotechnol.* **18**(1), 17–25 (2007).
5. T. Desmettre, J. Devoisselle, and S. Mordon, "Fluorescence properties and metabolic features of indocyanine green (ICG) as related to angiography," *Surv. Ophthalmol.* **45**(1), 15–27 (2000).
6. R. Philip, A. Penzkofer, W. Baumler, R. Szeimies, and C. Abels, "Absorption and fluorescence spectroscopic investigation of indocyanine green," *J. Photochem. Photobiol., A* **96**(1–3), 137–148 (1996).
7. J. Caesar, S. Shaldon, L. Chindussi, L. Guevara, and S. Sherlock, "The use of indocyanine green in the measurement of hepatic blood flow and as a test of hepatic function," *Clin. Sci.* **21**, 43–57 (1961).
8. G. Paumgartner, M. Probst, R. Kraines, and L. CM, "Kinetics of indocyanine green removal from the blood," *Ann. N.Y. Acad. Sci.* **170**(1), 134–147 (1970).
9. X. Wei, J. Rannels, and C. Lin, "Selective uptake of indocyanine green by reticulocytes in circulation," *Invest. Ophthalmol. Visual Sci.* **44**(10), 4489–4496 (2003).
10. J. M. Maarek, D. Holschneider, and J. Harimoto, "Fluorescence of indocyanine green in blood: intensity dependence on concentration and stabilization with sodium polyaspartate," *J. Photochem. Photobiol., B* **65**(2–3), 157–164 (2001).
11. X. Intes, J. Ripoll, Y. Chen, S. Nioka, A. Yodh, and B. Chance, "In vivo continuous-wave optical breast imaging enhanced with indocyanine green," *Med. Phys.* **30**(6), 1039–1047 (2003).
12. X. Li, B. Beauvoit, R. White, S. Nioka, B. Chance, and A. Yodh, "Tumor localization using fluorescence of indocyanine green (ICG) in a rat model," *Proc. SPIE* **2389**, 789–797 (1995).
13. J. Reynolds, T. Troy, R. Mayer, A. Thomson, D. Waters, K. Cornell, P. Snyder, and E. Sevick-Muracac, "Imaging of spontaneous canine mammary tumors using fluorescence contrast agents," *Photochem. Photobiol.* **70**(1), 87–94 (1999).
14. V. Ntziachristos, A. Yodh, M. Schnall, and B. Chance, "Concurrent MRI and diffuse optical tomography of breast after indocyanine green enhancement," *Proc. Natl. Acad. Sci. U.S.A.* **97**(6), 2767–2772 (2000).
15. C. Tung, "Fluorescent peptide probes for *in vivo* diagnostic imaging," *Biopolymers* **76**(5), 391–403 (2004).
16. K. J. Baker, "Binding of sulfobromophthalein (BSP) sodium and indocyanine green (ICG) by plasma alpha-1 lipoproteins," *Proc. Soc. Exper. Biol. Med. Soc. Exper. Biol. Med.* **122**(4), 957–963 (1966).
17. I. Fox and E. Wood, "Indocyanine green: physical and physiologic properties," *Proc. Staff Meet. Mayo Clin.* **35**(25), 732–744 (1960).
18. W. Holzer, M. Mauerer, A. Penzkofer, R. M. Szeimies, C. Abels, M. Landthaler, and W. Baumler, "Photostability and thermal stability of indocyanine green," *J. Photochem. Photobiol., B* **47**(2–3), 155–164 (1998).
19. V. Saxena, M. Sadoqi, and J. Shao, "Polymeric nanoparticulate delivery system for indocyanine green: biodistribution in healthy mice," *Int. J. Pharm.* **308**(1–2), 200–204 (2006).
20. K. Soppimath, T. Aminabhavi, A. Kulkarni, and W. Rudzinski, "Biodegradable polymeric nanoparticles as delivery devices," *J. Controlled Release* **70**(1–2), 1–20 (2001).
21. J. Panyam and V. Labhasetwar, "Biodegradable nanoparticles for drug and gene delivery to cells and tissue," *Adv. Drug Delivery Rev.* **55**(3), 329–347 (2003).
22. H. Maeda and Y. Matsumura, "Tumorotropic and lymphotropic principles of macromolecular drugs," *Crit. Rev. Ther. Drug Carrier Syst.* **6**(3), 193–210 (1989).
23. R. Duncan, "Polymer conjugates for tumour targeting and intracytoplasmic delivery. The EPR effect as a common gateway?" *Pharm. Sci. Technol. Today* **2**(11), 441–449 (1999).
24. V. Saxena, M. Sadoqi, and J. Shao, "Enhanced photo-stability, thermal-stability and aqueous-stability of indocyanine green in polymeric nanoparticulate systems," *J. Photochem. Photobiol., B* **74**, 29–38 (2004).
25. J. Yu, M. Yaseen, B. Anvari, and M. Wong, "Synthesis of near-infrared-absorbing nanoparticle-assembled capsules," *Chem. Mater.* **19**(6), 1277–1284 (2007).
26. F. Yuan, M. Dellian, D. Fukumura, M. Leunig, D. Berk, V. Torchilin, and R. Jain, "Vascular permeability in a human tumor xenograft: molecular size dependence and cutoff size," *Cancer Res.* **55**(17), 3752–3756 (1995).
27. E. Chernikova, P. Terpigova, C. Bui, and B. Charleux, "Effect of comonomer composition on the controlled free-radical copolymerization of styrene and maleic anhydride by reversible addition-fragmentation chain transfer (RAFT)," *Polymer* **44**(15), 4101–4107 (2003).
28. S. Henry, M. El-Sayed, C. Pirie, A. Hoffman, and P. Stayton, "pH-responsive poly(styrene-alt-maleic anhydride) alkylamide copolymers for intracellular drug delivery," *Biomacromolecules* **7**(8), 2407–2414 (2006).
29. J. Wong, T. Duhscherer, G. Pietraru, and D. Cramb, "Novel fluorescence spectral deconvolution method for determination of critical micelle concentrations using the fluorescence probe PRODAN," *Langmuir* **15**(19), 6181–6186 (1999).
30. S. Harrisson and K. Wooley, "Shell-crosslinked nanostructures from amphiphilic AB and ABA block copolymers of styrene-alt-(maleic anhydride) and styrene: polymerization, assembly and stabilization in one pot," *Chem. Commun. (Cambridge)* **26**, 3259–3261 (2005).
31. M. Q. Zhu, L. H. Wei, F. S. Du, Z. C. Li, F. M. Li, M. Li, and L. Jiang, "A unique synthesis of a well-defined block copolymer having alternating segments constituted by maleic anhydride and styrene and the self-assembly aggregating behavior thereof," *Chem. Commun. (Cambridge)* **4**, 365–366 (2001).

32. A. Lavasanifar, J. Samuel, and G. Kwon, "Poly(ethyl oxide)-block-poly(L-amino acid) micelles for drug delivery," *Adv. Drug Delivery Rev.* **54**(2), 169–190 (2002).
33. R. Rajagopalan, P. Uetrecht, J. Bugaj, S. Achilefu, and R. Dorshow, "Stabilization of the optical tracer agent indocyanine green using noncovalent interactions," *Photochem. Photobiol.* **71**(3), 347–350 (2000).
34. Z. Sezgin, N. Yuksel, and T. Baykara, "Preparation and characterization of polymeric micelles for solubilization of poorly soluble anti-cancer drugs," *Eur. J. Pharm. Biopharm.* **64**(3), 261–268 (2006).
35. C. Zhang, Y. Ding, L. Yu, and Q. Ping, "Polymeric micelle systems of hydroxycamptothecin based on amphiphilic *N*-alkyl-*N*-trimethyl chitosan derivatives," *Colloids Surf.* **55**(2), 192–199 (2007).
36. R. Vakil and G. Kwon, "Poly(ethylene glycol)-b-poly(ϵ -caprolactone) and PEG-phospholipid form stable mixed micelles in aqueous media," *Langmuir* **22**(23), 9723–9729 (2006).
37. C. Giacomelli, L. Le Men, R. Borsali, J. Lai-Kee-Him, A. Brisson, S. Armes, and A. Lewis, "Phosphorylcholine-based pH-responsive diblock copolymer micelles as drug delivery vehicles: light scattering, electron microscopy, and fluorescence experiments," *Biomacromolecules* **7**(3), 817–828 (2006).
38. W. Shim, S. Kim, E. K. Choi, H. J. Park, J. S. Kim, and D. Lee, "Novel pH sensitive block copolymer micelles for solvent free drug loading," *Macromol. Biosci.* **6**(2), 179–186 (2006).
39. Sigma-Aldrich, "Material safety data sheet—Tetrabutylammonium iodide," Sigma-Aldrich, Milwaukee, WI (2006).
40. Y. Chang, R. Prange, H. Allcock, S. Lee, and C. Kim, "Amphiphilic poly[cbis(trifluoroethoxy)phosphazene]-poly(ethylene oxide) block copolymers: synthesis and micellar characteristics," *Macromolecules* **35**(22), 8556–8559 (2002).
41. C. L. Lo, C. K. Huang, K. M. Lin, and G. H. Hsiue, "Mixed micelles formed from graft and diblock copolymers for application in intracellular drug delivery," *Biomaterials* **28**(6), 1225–1235 (2007).
42. S. La, T. Okano, and K. Kataoka, "Preparation and characterization of the micelle-forming polymeric drug indomethacin-incorporated poly(ethylene oxide)-poly(β -benzyl-L-aspartate) block copolymer micelles," *J. Pharm. Sci.* **85**(1), 85–90 (1996).
43. S. Patwardhan, S. Bloch, S. Achilefu, and J. Culver, "Time-dependent whole-body fluorescence tomography of probe bio-distributions in mice," *Opt. Express* **13**(7), 2564–2577 (2005).